Performance and robustness trade-off capabilities for the VEGA launcher TVC system

Diego Navarro-Tapia[⋆†], *Andrés Marcos*[⋆], *Samir Bennani* [⋆⋆] *and Christophe Roux*[⋆⋆⋆]
[⋆] *University of Bristol, Technology for AeroSpace Control (TASC) Lab.,*
Bristol, BS8 1TR, United Kingdom;
e-mail: diego.navarro-tapia@bristol.ac.uk · andres.marcos@bristol.ac.uk
[⋆⋆] *ESA-ESTEC,*
Noordwijk, 2201AZ, The Netherlands; e-mail: samir.bennani@esa.int
[⋆⋆⋆] *AVIO, VEGA GNC Department,*
Colleferro, 00034, Italy; e-mail: christophe.roux@avio.com
[†]Corresponding author

Abstract

This article presents a methodological synthesis framework based on the structured $\mathcal{H}_\infty$ approach for the design of atmospheric launcher TVC systems, using the VEGA launcher as the application case. The main advantage of this framework is that the TVC design can be recast into a formal multi-objective optimisation problem in which robust stabilisation, disturbance rejection and performance minimisation are managed in a simultaneous fashion. This article illustrates how the proposed framework can be guided to favour a specific trade-off performance objective via proper choice of the design weighting functions. The capabilities to manage different control strategies are demonstrated via several structured $\mathcal{H}_\infty$ designs which are tailored to maximise specific performance metrics (i.e. loads, drift, attitude errors). These controllers are analysed and compared through high-fidelity, nonlinear time-domain Monte Carlo simulations of the VEGA atmospheric flight.

1. Introduction

This paper addresses the design of the atmospheric ascent-flight control system of the VEGA launcher Thrust Vector Control (TVC) system. In this phase, the launch vehicle is heavily impacted by loads coming from high dynamic pressure during the flight as well as strong, dynamic control deflections and changes in the angle of attack. In addition, the launch vehicle exhibits a flexible behaviour characterised by several resonant modes that can generate large oscillations and lead to instability. Despite all these difficulties, the control system must ensure stability to guidance commands while satisfying very demanding and tight performance requirements in the presence of parameter dispersions and external disturbances.

Based on the above, the atmospheric ascent-flight of a launch vehicle represents a very challenging control problem, which is traditionally addressed using a classical design approach. In this article, this rich heritage from classical control is used to recast the TVC control design problem into a systematic robust control synthesis framework based on the structured $\mathcal{H}_\infty$ approach.[1,2] This synthesis technique allows to manage classical control architectures in a robust fashion by means of performing an $\mathcal{H}_\infty$ optimisation while enforcing a specific controller structure and/or state order. The capability of defining the controller structure for design is very advantageous for many industrial applications, and as detailed in the works of Ganet-Schoeller et al[8] and Simplício et al,[17] it is particularly well suited for launcher TVC design of already existing and future expendable and reusable launch vehicles.

The proposed framework is oriented to simultaneously handle multiple performance requirements, and as demonstrated in the work of Navarro-Tapia et al,[14] it has the capability to enhance wind disturbance rejection properties and to explicitly include system parametric uncertainties in the design. In addition, unlike the state-of-practice, the proposed formulation allows to optimise the rigid-body controller and bending filter in one single procedure (as demonstrated in the work of Navarro-Tapia et al[13]). Thus, this design scheme can significantly simplify the state-of-practice for TVC design and reduce tuning effort across launch missions while keeping, and indeed simplifying, the classical VEGA TVC architecture.

The main aim of this article is to reconcile all the aforementioned aspects and show how this robust control synthesis framework can be formulated to steer the design for different competing trade-off performance objectives (e.g. structural loads, drift, attitude error) while achieving stability robustness throughout the atmospheric flight. The management of launcher design trade-offs is traditionally performed, as exemplified in the works of Suzuki[18] and Wie et al,[19] using classical control principles (also known as Hoelker's conditions[9]). In this paper, this is illustrated via several structured $\mathcal{H}_\infty$ design examples which are performed to favour a specific requirement. These designs are then compared and analysed using high-fidelity, nonlinear time-domain simulations.

This paper is organised as follows. Section 2 describes the VEGA launcher, its atmospheric phase GNC architecture and the uncertain vehicle model used for design. Subsequently, in Section 3, the atmospheric VEGA TVC system design is formulated as a structured $\mathcal{H}_\infty$ control problem and three different designs are performed for distinct, and competing, control objectives. Section 4 analyses the resulting structured $\mathcal{H}_\infty$ controllers via nonlinear Monte Carlo simulations. And finally, Section 5 provides the conclusions of this paper.

2. VEGA launcher

This section introduces first the VEGA launch vehicle and its atmospheric phase GNC architecture (sub-section 2.1). In addition, the uncertain Linear Fractional Transformation (LFT) vehicle model employed for design is briefly described in sub-section 2.2.

2.1 VEGA launcher vehicle and atmospheric flight

VEGA (*Vettore Europeo di Generazione Avanzata*) is the smallest European launcher with approximately 30 m in height and a diameter of 3 m. This launch vehicle has been developed under the responsibility of the European Space Agency (ESA) and AVIO SpA as prime contractor. VEGA addresses the small and mini-satellites market (payloads from 300 kg to 2500 kg), and performs a wide range of missions for Earth observation satellites and many specific purposes using mainly Sun-synchronous and low Earth orbits. The launcher has successfully performed fourteen launches since its maiden flight on 13^{th} February 2012 (all of them from the VEGA launch site located in Guiana Space Centre – Kourou, France).

VEGA is a single-body launcher that follows a four-stage approach (see Figure 1). The three first stages are formed by three solid propellant motors (P80, Zefiro 23 and Zefiro 9), whereas the 4^{th} stage, also known as Attitude and Vernier Upper Module (AVUM), is composed of a bi-propellant liquid engine that provides fine attitude control capability and accurate payload orbital insertion. The liquid motor of the AVUM stage can be re-ignited to perform several boosts providing the capability to place multiple payloads into orbit as well as a de-orbiting boost.

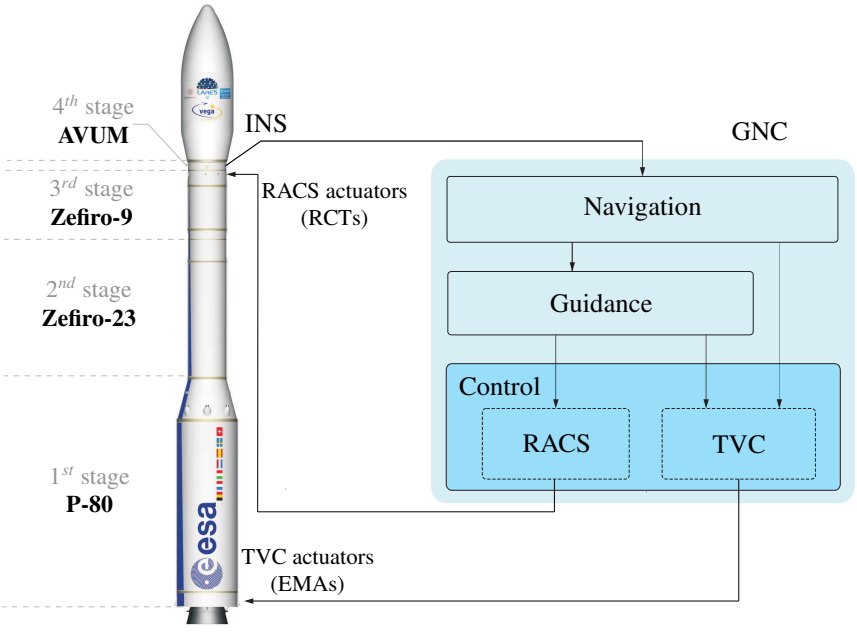

Figure 1: VEGA launcher description and GNC architecture

Figure 1 also illustrates the Guidance, Navigation and Control (GNC) scheme of the VEGA launcher. The control architecture is composed of a TVC system and a Roll Attitude Control System (RACS). The former provides pitch and yaw attitude control for all stages by generating the necessary nozzle deflections using two orthogonal Electro-Mechanical Actuators (EMAs) (termed as lane A and B), while the latter performs roll attitude control using six on/off Reaction Control Thrusters (RCTs) located at the AVUM.

The focus of this article is on the ascent-atmospheric flight (1^{st} stage) of the mission. It is important to mention that during the first stage the guidance function is performed in open-loop following a pre-programmed trajectory based on attitude tables versus a scheduling variable (i.e. time or velocity). The reason is that a closed-loop guidance configuration could potentially lead to critical angles of attack resulting in unacceptable aerodynamic loads due to the effect of wind disturbance. Thus, with the guidance following an open-loop configuration, the GNC system must perform a pseudo-guidance role by keeping the launcher close to its reference trajectory while also limiting structural loads. This control task is particularly challenging because of the competing nature of the multiple objectives required to achieve during the atmospheric flight. Subsequently, any final resulting deviations from the nominal reference trajectory are corrected during the upper stages using closed-loop guidance.

Another special feature of the first stage is that the roll rate is only limited, which means that the RACS will only act if the roll rate is over a certain threshold. The main reason is that the RCTs are not strong enough to set the roll rate to zero due to the high moment of inertia that the launch vehicle exhibits during the atmospheric flight and the high dynamic pressure of the environment. In fact, telemetry from real flights show that there are typically no RCT activations during the first stage.[5]

It is noted that all the simulations and designs in this article are performed using the actual VEGA 5^{th} flight mission (VV05) data.[3] The payload of this mission was the Sentinel-2A satellite.

2.2 Launch vehicle model

The motion of a launch vehicle is described by the standard 6 Degrees of Freedom (DoF) equations of motion, which represent the translational and rotational dynamics of the vehicle. The VEGA launcher presents axial symmetry about the roll axis, and thus, considering a negligible roll rate, the pitch and yaw axes can be considered decoupled and more importantly identical. This is a standard assumption in launch vehicle TVC synthesis that allows to perform the design and analysis in a single plane (pitch or yaw axis). In particular, this article focuses on the yaw axis.

All relevant dynamics are typically expressed with the state-space representation shown in Equation 1, where the contributions of the rigid- and flexible-body dynamics are denoted separately by subscripts R and F respectively. The reader is referred to the work of Navarro-Tapia et al[14] for further details on the derivation of the equations of motion and the definition of the state-space matrices in Equation 1.

The launch vehicle model $G_{LV_{RF}}(s)$ given in Equation 1 contains the main rigid-body rotational and translational dynamics due to thrust and aerodynamics and the nozzle dynamics also known as Tail-Wags-Dog (TWD) effect. The elastic behaviour of the launch vehicle is characterised by several bending modes represented by a 2^{nd} order model with low damping. In addition, other contributions such as sensors characterization and wind disturbance dynamics are also considered. $G_{LV_{RF}}(s)$ uses four rigid-body states given by the drift z, yaw attitude angle ψ and their derivatives ($\mathbf{x_R} = [z\ \dot{z}\ \psi\ \dot{\psi}]^T$); two flexible-body states accounting for the first bending mode ($\mathbf{x_F} = [q_1\ \dot{q}_1]^T$); five outputs ($\mathbf{y_{LV}} = [Q\alpha\ \psi_{INS}\ \dot{\psi}_{INS}\ z_{INS}\ \dot{z}_{INS}]^T$), which include the load performance indicator $Q\alpha$ (with Q the dynamic pressure and α the angle of attack) and the measurements at INS node location for the four rigid-body states; and three inputs ($\mathbf{u_{LV}} = [\beta_\psi\ \ddot{\beta}_\psi\ v_w]^T$), with β_ψ the nozzle deflection angle and v_w the wind velocity.

$$\underbrace{\begin{aligned}\begin{bmatrix}\dot{\mathbf{x_R}}\\ \dot{\mathbf{x_F}}\end{bmatrix} &= \begin{bmatrix}A_R & A_{RF}\\ A_{FR} & A_F\end{bmatrix}\begin{bmatrix}\mathbf{x_R}\\ \mathbf{x_F}\end{bmatrix} + \begin{bmatrix}B_R\\ B_F\end{bmatrix}\mathbf{u_{LV}}\\ \mathbf{y_{LV}} &= \begin{bmatrix}C_R & C_F\end{bmatrix}\begin{bmatrix}\mathbf{x_R}\\ \mathbf{x_F}\end{bmatrix} + D_R\ \mathbf{u_{LV}}\end{aligned}}_{G_{LV_{RF}}(s)} \tag{1}$$

For design and analysis purposes, the launch vehicle state-space model of Equation 1 can be used to derive nominal Linear Time Invariant (LTI) models at different operating points along the atmospheric phase considering that the parameters are frozen in time. Unfortunately, the launch vehicle system is inherently uncertain. In particular, vehicle mass, centre of gravity position and inertia, as well as bending mode frequencies and structural modal parameters are very difficult to estimate, and thus, an expected variability on those parameters must be accounted for in the synthesis. This can be addressed by using LFT theory[6] which allows to capture the uncertain behaviour of a system.

The LFT model of the VEGA launcher is derived by augmenting the LTI nominal models obtained from Equation 1 with additive parametric uncertainties using MATLAB's Robust Control Toolbox.[4] The reader is referred to references Marcos et al[11] and Navarro-Tapia et al[14] for further details on the LFT modelling approach used and on the list of uncertain parameters employed. The VEGA LFT model can be represented, see Figure 2a, as the upper LFT interconnection of the nominal model $G_{LV_{RF}}(s)$ subject to a set of rigid- and flexible-body uncertainties $\Delta_{LV_{RF}}$. The effect of the considered uncertainties on the launch vehicle model is illustrated in Figure 2b, which shows the frequency response of the nominal VEGA attitude channel at the flight instant t=50 s (in red) and 1000 random

scattered responses. This plot allows visualizing the range of uncertainty defined for the launch vehicle model for the rigid (inset of the left-side in same plot) and flexible (right-side part of Figure 2b) components.

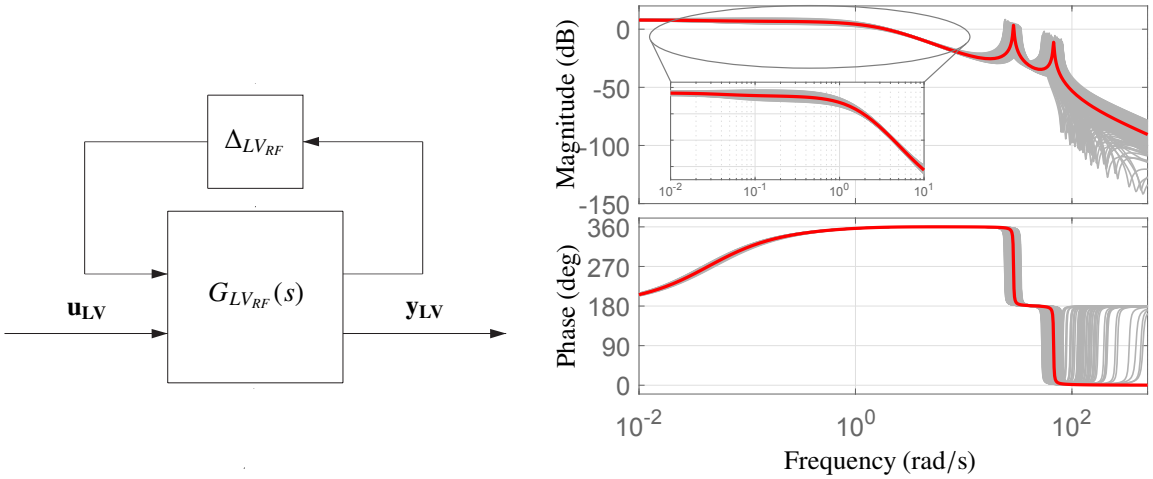

(a) VEGA LFT representation

(b) Bode plots of the attitude channel $\psi_{INS}/\beta_{\psi}(s)$ at t=50 s

Nominal response Scattered responses

Figure 2: Uncertain launch vehicle model

Furthermore, the delays originated by the on-board computer and the TVC actuator dynamics are also modelled as LFT representations (see Figure 3). Again, reference Navarro-Tapia et al[14] provides further details on the delay model while the work of Simplício et al[16] on the TVC LFT model.

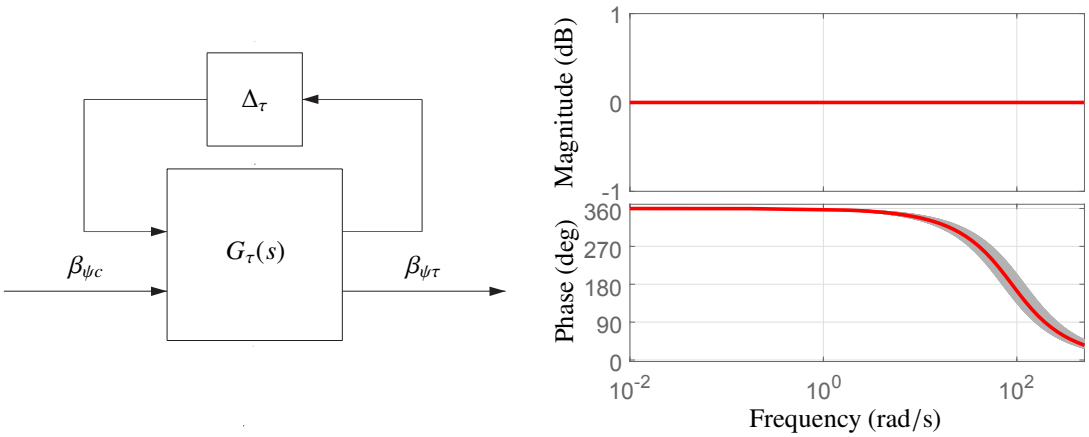

(a) Delay LFT representation

(b) Bode plots of the delay LFT model ($\beta_{\psi\tau}/\beta_{\psi c}(s)$)

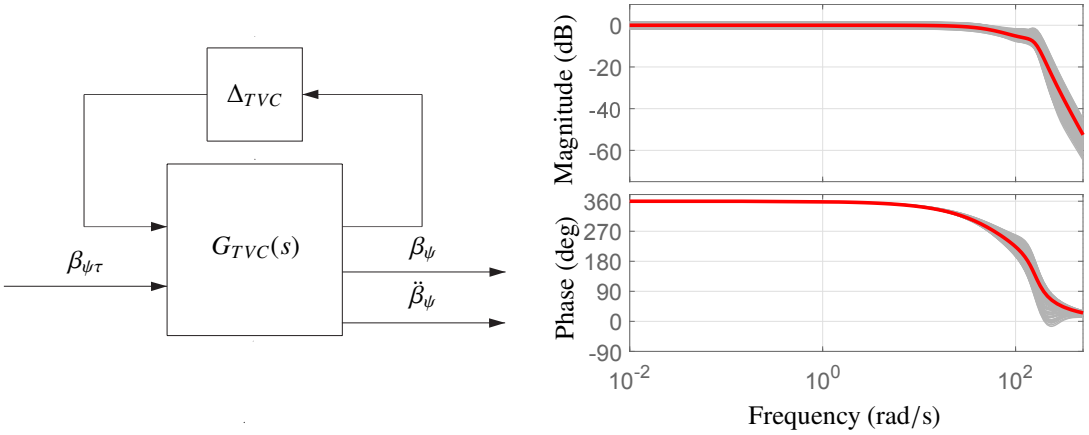

(c) TVC LFT representation

(d) Bode plots of the TVC LFT model ($\beta_{\psi}/\beta_{\psi\tau}(s)$)

Nominal response Scattered responses

Figure 3: Uncertain actuation chain models

3. Robust structured TVC synthesis

This section is dedicated to illustrate how the atmospheric VEGA TVC system design can be tailored for different competing trade-off performance objectives (e.g. attitude error, lateral deviations or structural loads) using a robust control synthesis framework based on the structured $\mathcal{H}_\infty$ technique.[1,2]

First, the different atmospheric trade-off design objectives are presented in sub-section 3.1. Then, in sub-section 3.2, the atmospheric VEGA TVC system design is formulated as a robust control problem using the structured $\mathcal{H}_\infty$ synthesis technique. Sub-section 3.3 describes how the different design strategies can be expressed in suitable frequency-domain weighting functions, and finally, three structured $\mathcal{H}_\infty$ TVC designs are presented and analysed in sub-section 3.4.

3.1 TVC design objectives for the atmospheric flight

The design of the atmospheric TVC system for a launch vehicle is typically performed at different linear design points along the atmospheric flight in order to cope with the large dynamical system variations (for example, the VEGA launcher uses 12 linear design sets at approximately every 10 s except at lift- and tail-off phases). These linear designs are then discretised and linearly scheduled versus the non-gravitational velocity.

The design of each of the linear controllers must fulfil simultaneously a set of different conflicting trade-off objectives. These linear designs are traditionally performed to favour one performance metric over the others depending on the flight phase (e.g. a load-relief control mode is generally employed around the maximum dynamic pressure region). These competing objectives can broadly be divided into the following three design strategies:

- Tracking: the control system will minimise the attitude deviations from the guidance commands at the exchange of presenting higher lateral deviations. In addition to the allowed lateral deviations, this strategy could potentially lead to high wind-induced structural loads.
- Drift: this design scheme aims at minimising the lateral deviations of the vehicle. In this case, the control system will attempt to generate an attitude response so that the normal forces are cancelled out. The drawbacks of this approach are attitude deviations and, as in the previous case, potentially high structural loads.
- Structural loads: the main objective of this approach is to minimise the wind-induced structural loads. The structural load performance metric $Q\alpha$ is given as follows (where V is the vehicle's velocity):

$$Q\alpha = Q(\psi + \frac{\dot{z}}{V} - \frac{v_w}{V}) \tag{2}$$

  This design strategy will turn the vehicle into the wind to reduce the angle of attack. By looking at Equation 2, this can be done by minimising the wind contribution on the attitude and drift-rate channels.

This performance trade-off problem is generally oriented towards minimising the performance degradation due to the wind disturbance. In fact, the main traditional launcher control strategies[9] considered in the literature aim to cancel out the steady-state values of each of the previous three performance metrics from the wind disturbance input. Unfortunately, as shown in the work of Navarro-Tapia et al,[14] only the steady-state value of the drift-wind channel can be minimised using the current TVC architecture of the VEGA launcher. Despite this control architecture limitation, it is possible to improve the wind disturbance rejection performance of VEGA by focusing on the transient response and more importantly, it can be steered to prioritise one performance metric over the others as it will be shown in this section.

3.2 Synthesis interconnection

The control design problem is formulated as the closed-loop interconnection shown in Figure 4. This diagram has a set of inputs formed by commands, wind disturbance and sensor noise inputs, and a set of outputs formed by the attitude error ψ_e, the commanded actuator deflection $\beta_{\psi c}$, the load performance metric $Q\alpha$, and the INS measurements for attitude ψ_{INS}, drift z_{INS} and drift-rate $\dot{z}_{INS}$. Note that the input-output channels are scaled by frequency-domain weighting functions (represented by gray-shaded blocks) to specify the control design objectives. The selection of these weighting functions will be discussed later in sub-section 3.3.

In addition to the weighting functions, this closed-loop diagram contains the three LFT models presented in sub-section 2.2 (i.e. launch vehicle model, delay and TVC actuator), a turbulence wind model $G_w(s)$ that will be described in sub-section 3.2.1, and finally the tunable controller $K_{RF}(s)$ (highlighted with a blue box) that will be presented in sub-section 3.2.2.

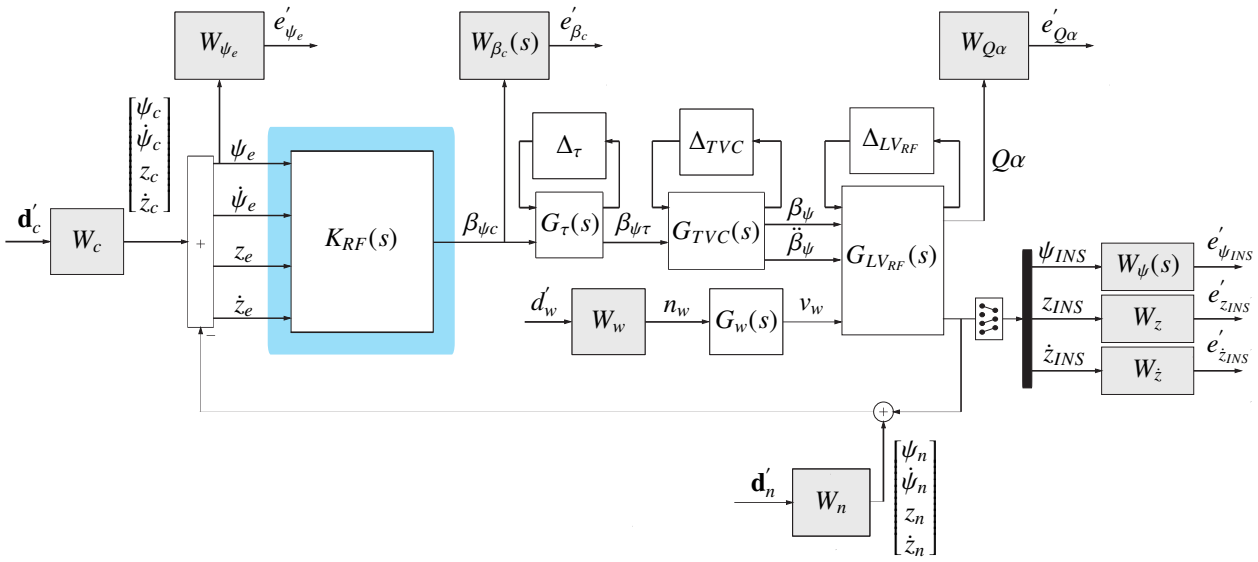

Figure 4: Closed-loop diagram for the joint design of VEGA's rigid-body controller and bending filter

3.2.1 Wind generator $\mathbf{G_w(s)}$

The effect of wind disturbance is a critical factor for any launcher atmospheric phase.[12] It generally produces a significant degradation in the global performance of the mission and it induces structural loads that can cause loss of vehicle. Although this is critically important, especially for launchers, only a few instances in the aerospace domain can be found where this is directly employed in the launcher design process.

To overcome this problem, a wind turbulence model $G_w(s)$ is placed at the wind disturbance input of the launch vehicle model (see Figure 4). The main aim with this addition is to provide the structured $\mathcal{H}_\infty$ optimiser with information about the statistical wind levels that the launch vehicle will encounter along the atmospheric flight. Indeed, in reference Navarro-Tapia et al,[14] it is shown that the use of strong wind turbulence levels for design significantly contributes to improve the wind disturbance rejection performance of the system.

$G_w(s)$ is based on the Dryden filter given in Equation 3, which defines the wind disturbance velocity v_w from an unitary white noise input n_w. This wind model configuration has been obtained following the criteria from the work of Johnson[10] and the model description given in Simplício et al.[16]

$$G_w(s) = \frac{v_w(s)}{n_w(s)} = \frac{\sqrt{\frac{2}{\pi}\frac{V - v_{wp}(h)}{L_h}\sigma_h^2}}{s + \frac{V - v_{wp}(h)}{L_h}} \tag{3}$$

in the above model L_h and σ_h are the turbulence length scale and the standard deviation of the wind turbulence. The values for these parameters can be found in tabular-form for light, moderate and severe turbulence levels versus altitude h in reference.[10] On the other hand, $v_{wp}(h)$ defines the vertical profile of wind velocity.

3.2.2 Tunable controller $\mathbf{K_{RF}(s)}$

The architecture of the tunable controller $K_{RF}(s)$ is shown in Figure 5. The controller receives as inputs the yaw attitude error ψ_e and its rate $\dot{\psi}_e$, and the lateral deviations (both in position z_e and velocity $\dot{z}_e$) with respect to the reference trajectory and calculates the required yaw nozzle deflection $\beta_{\psi c}$ to follow the guidance commands.

The structure of $K_{RF}(s)$ is based on the actual VEGA TVC control system architecture.[15] It is composed of a rigid-body controller and a bending filter $H_3(s)$. As it will be discussed later, these two parts of $K_{RF}(s)$ are first parametrised as a function of tunable parameters for design and then optimised simultaneously using the structured $\mathcal{H}_\infty$ framework.

Tunable rigid-body controller

The rigid-body control law is based on a classical structure formed by a Proportional-Derivative (PD) controller on attitude $(K_{\psi p}, K_{\psi d})$ to stabilise and control the rigid-body launch vehicle, and a lateral control feedback composed of a PD controller on drift $(K_z, K_{\dot{z}})$ to limit the lateral deviations of the vehicle and minimise the angle of attack for loads alleviation.

In preparation for the subsequent structured $\mathcal{H}_\infty$ optimisation, these four rigid-body gains are configured as tunable parameters with no constraints on their allowable values.

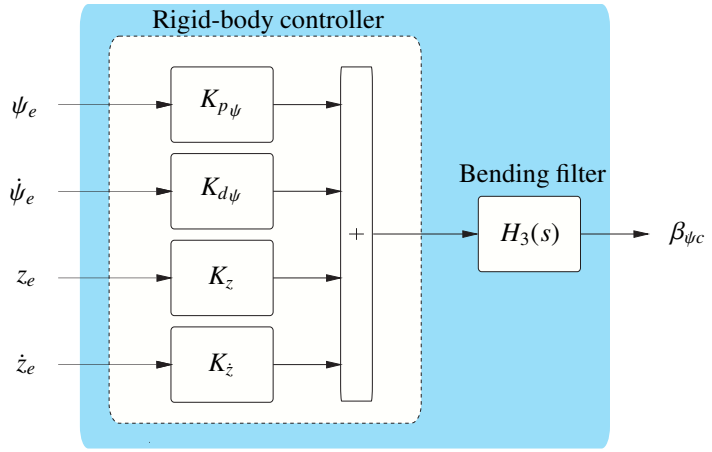

Figure 5: Tunable controller $K_{RF}(s)$

Tunable bending filter

The TVC system must also ensure that the bending modes (BMs) related to the flexible structure of the launch vehicle are not excited. This is traditionally performed using a set of filters, also known as bending filters, that provide stabilisation against the flexible modes. In this work, the bending filter $H_3(s)$ (see Figure 5) uses the same structure as that of reference Navarro-Tapia et at,[13] which is briefly described next.

The bending filter $H_3(s)$ is parametrised as in Equation 4. The proposed factorisation was obtained based on system physical knowledge (such as the use of notch filters to phase stabilise the first bending mode) to yield a general bending filter configuration. In particular, $H_3(s)$ is factorised into four 2^{nd}-order notch filters and one 6^{th}-order low-pass filter. The first notch filter is centred at $\underline{\omega_{q_1}}$, which is the minimum expected dispersed frequency of the 1^{st} bending mode due to uncertainties. Following this notation, the other notch filters are centred at the nominal and maximum frequencies of the 1^{st} bending mode (ω_{q_1} and $\overline{\omega_{q_1}}$) and at $\underline{\omega_{q_2}}$, which is the minimum expected frequency for the 2^{nd} bending mode. Finally, the low-pass filter provides attenuation for the upper modes.

$$H_3(s) = \underbrace{\prod_{i=1}^{4} \frac{s^2 + \eta_i s + (\omega_i')^2}{s^2 + \eta_i/\epsilon_i s + (\omega_i')^2}}_{\text{Notch filters}} \cdot \underbrace{\left(\frac{\epsilon_{LP} s^2 + \eta_{LP} s + (0.6\omega_{q_2}')^2}{s^2 + \eta_{LP} s + (0.6\omega_{q_2}')^2} \right)^3}_{\text{Low-pass filter}} \tag{4}$$

$$\begin{aligned} \omega_1 &= \underline{\omega_{q_1}}\ [\min 1^{st} BM] \\ \omega_2 &= \omega_{q_1}\ [\text{nom} 1^{st} BM] \\ \omega_3 &= \overline{\omega_{q_1}}\ [\max 1^{st} BM] \\ \omega_4 &= \underline{\omega_{q_2}}\ [\min 2^{nd} BM] \end{aligned} \qquad \text{[Upper BMs attenuation]}$$

It is important to remark here that all the frequency parameters in Equation 4 are pre-warped before design to minimise the distortion caused by the discretisation process.[13] The following bilinear Tustin transformation is employed here:

$$\omega' = \frac{\omega_p}{\tan(\omega_p T_s/2)} \tan(\omega T_s/2) \tag{5}$$

with the nominal 1^{st} bending mode frequency as warping frequency ($\omega_p = \omega_{q_1}$) and T_s the sampling rate.

The proposed configuration in Equation 4 results in 10 tunable parameters for $H_3(s)$. In order to reduce the tunable parameters and also simplify the control optimisation, the structured $\mathcal{H}_\infty$ approach allows to define a priori which parameters are to be tuned and which ones can be fixed for the optimisation. In addition, it is also possible to constraint the optimisation by defining minimum and maximum allowable values for each tunable coefficient. In this sense, the design configuration used here is shown in Table 1. It can be seen that the parameters related to the low-pass filter and the width of the notch filters (η_i) are fixed, whereas the attenuation at the center frequency of the notch filters (ϵ_i) are defined as tunable parameters. This configuration results in four tunable parameters.

Table 1: Structured $\mathcal{H}_\infty$ configuration for the tunable bending filter $H_3(s)$

	Fixed parameters		**Tunable parameters**		
Filter	*Parameter*	*Value*	*Parameter*	*min*	*max*
Notch filter 1	η_1	2	ϵ_1	-25 dB	-10 dB
Notch filter 2	η_2	5	ϵ_2	-10 dB	-4 dB
Notch filter 3	η_3	2	ϵ_3	-25 dB	-10 dB
Notch filter 4	η_4	12	ϵ_4	-20 dB	-15 dB
Low-pass filter	η_{LP}	40			
	ϵ_{LP}	-25/3 dB			

3.3 Weighting function selection

In this subsection, the selection of the weighting functions for three different control strategies (i.e. attitude, load and drift) is discussed.

The three designs use the same input weighting functions given in Equation 6. It is remarked that these values are the same employed in reference.[13] Note that all the input weights are constant functions and that the weights corresponding to the wind disturbance and the sensor noise inputs (W_w and W_n) are kept fixed for all the linear design points throughout the atmospheric flight. This choice is made to consider an unitary white noise input n_w with 3 standard deviation and the same sensor noise for all the linear points.

$$\begin{aligned} W_c &= diag\Big(\frac{\pi}{180}, [1-2.6]\frac{\pi}{180}, [5-30], 1\Big) \\ W_w &= 3 \\ W_n &= diag\Big(0.02\frac{\pi}{180}, 0.1\frac{\pi}{180}, 0.01, 0.001\Big) \end{aligned} \tag{6}$$

As for the output weighting functions, the three designs use the same weight configuration but with different values for each design. This setup is described in Equation 7.

$$\begin{aligned} W_\psi(s) &= \tfrac{180}{\pi}\Big(\frac{h_\psi s+\omega_\psi}{s+\omega_\psi/l_\psi}\Big)^{-1}; & W_z &= \Big(z_{max}\Big)^{-1}; & W_{Q\alpha} &= \tfrac{180}{\pi}\Big(\alpha_{max}Q\Big)^{-1}; \\ W_{\psi_e} &= \tfrac{180}{\pi}\Big(l_\psi\Big)^{-1}; & W_{\dot z} &= \Big(\dot z_{max}\Big)^{-1}; & W_{\beta_c}(s) &= \tfrac{180}{\pi}\Big(l_u H_3(s)\Big)^{-1} \end{aligned} \tag{7}$$

Briefly, the inverse of $W_\psi(s)$ is chosen as a low-pass filter to limit the complementary sensitivity function of the attitude channel, with l_ψ and h_ψ as the low- and high-frequency asymptotes and ω_ψ as the filter bandwidth. ω_ψ is fixed to 10 rad/s and h_ψ to -40 dB for each of the three control strategies and for all the linear design points. Differently, l_ψ is varied as shown in Table 2 to address each specific requirement (i.e. attitude, drift and load). On the other hand, the attitude sensitivity function is weighted by $W_{\psi_e}^{-1}$, which is defined here as a constant weighting function depending on the aforementioned l_ψ.

The lateral control requirements are specified by W_z and $W_{\dot z}$, whose inverses refer to the maximum drift z_{max} and drift-rate $\dot z_{max}$ expected values. In addition, $W_{Q\alpha}^{-1}$ enforces a maximum angle of attack α_{max}. The range of values taken by z_{max}, $\dot z_{max}$ and α_{max} are given in Table 2 for each of the control design strategies.

Finally, the weighting function $W_{\beta c}(s)$ is expressed as a function of a constant parameter l_u and the bending filter factorisation $H_3(s)$ given in Equation 4. This formulation allows to impose the desired frequency response for the bending filter design. For ease of simplicity, the same weight values of $W_{\beta c}(s)$ employed in reference[13] are used here for the three different control strategies.

Table 2: Trade-off tuning for the output weighting functions

	Attitude controller	Drift controller	Load controller
l_ψ (dB)	5	15	5
z_{max} (m)	[3000-5000]	[10-100]	[30-200]
$\dot z_{max}$ (m/s)	[15-100]	[10-15]	[2-3]
α_{max} (deg)	10	10	[1.5-3]

Table 2 quantifies the rationale for each of the designs. For example, the main rationale behind the attitude controller is to let the vehicle drift with respect to the reference trajectory (see high values for z_{max} and $\dot{z}_{max}$) and to impose a low value for l_ψ to limit the wind contribution in the attitude channel. Note also that, this control strategy does not penalise the structural load performance (see the high value for α_{max}). A different approach is followed to design the drift controller. In this case, the control effort is made to reduce the drift of the vehicle (by imposing low values for z_{max} and $\dot{z}_{max}$) at the exchange of worsening the tracking performance (by setting a higher value for the low-frequency asymptote l_ψ). Similarly as for the attitude scheme, the structural load performance is not penalised here (α_{max} = 10 deg). And finally, for the load strategy the proposed design formulation allows to address this scheme in a twofold manner. The most explicit one is by setting a low maximum angle of attack (i.e. $\alpha_{max} = [1.5 - 3]$deg). The second one is based on the dependency of the structural load metric $Q\alpha$ on attitude tracking and drift-rate (see Equation 2). This dual dependency is tackled by enforcing low values for the low-frequency asymptote l_ψ and for the maximum drift-rate $\dot{z}_{max}$. In this instance, the maximum drift z_{max} takes higher values with respect to the drift controller case to favour the attitude tracking performance.

It is important to remark here that the level of performance of the three atmospheric designs is limited by the classic trade-off between stability robustness and performance. This means that the selection of the above weighting functions was performed not only in trying to favour the specific design requirement but also considering the aforementioned underlying limitation to guarantee satisfactory stability margins under dispersed conditions (i.e. 3 dB low- and high-frequency gain margins and 40 ms delay margin).

3.4 Robust structured control synthesis

For each of the previous three control design strategies, 8 linear controllers are synthesised at every 10 seconds between the flight instants t=20 s and t=90 s using the structured $\mathcal{H}_\infty$ technique. All these linear controllers are constrained by the structural limitations defined in sub-section 3.2.2. The structured $\mathcal{H}_\infty$ optimisation is formulated with the weighting functions described in sub-section 3.3 using Matlab's Robust Control Toolbox *hinfstruct* function.[7] It is important to remark here that the control problem is set to perform multiple optimisations from a set of 5 random initialisations to mitigate the local-minima nature of the structured $\mathcal{H}_\infty$ approach.

To evaluate the performance of the three different control strategies (i.e. attitude, drift and load), the frequency responses of the attitude, drift and $Q\alpha$ channels from the wind disturbance input n_w are shown in Figure 6 for the linear design point obtained at t=50 s (i.e. around maximum dynamic pressure). The figure shows 500 dispersed random LFT samples (the same samples are used for the three controllers).

By looking at Figure 6a, it is noted that the attitude controller (in green) provides better wind disturbance rejection (i.e. lower values) for the attitude channel than the other two controllers. This feature is easily seen at low frequencies between 0.001 and 0.1 rad/s. As expected, the drift controller (in red) is the one providing worst tracking performance with respect to wind featuring very high amplitudes around 0.4 rad/s.

Figure 6b clearly illustrates the trade-off between tracking and lateral deviation. Note that the trend here is the opposite with respect to Figure 6a. It is very noticeable that the drift controller (in red) is the one that exhibits lower values, whereas the attitude controller (in green) presents very high values at low frequencies. This means that the drift controller will provide better wind rejection performance for the drift channel, as expected. Note also that as shown in reference,[14] the steady-state value of the drift-wind channel can be controlled using the current control architecture of the VEGA launcher.

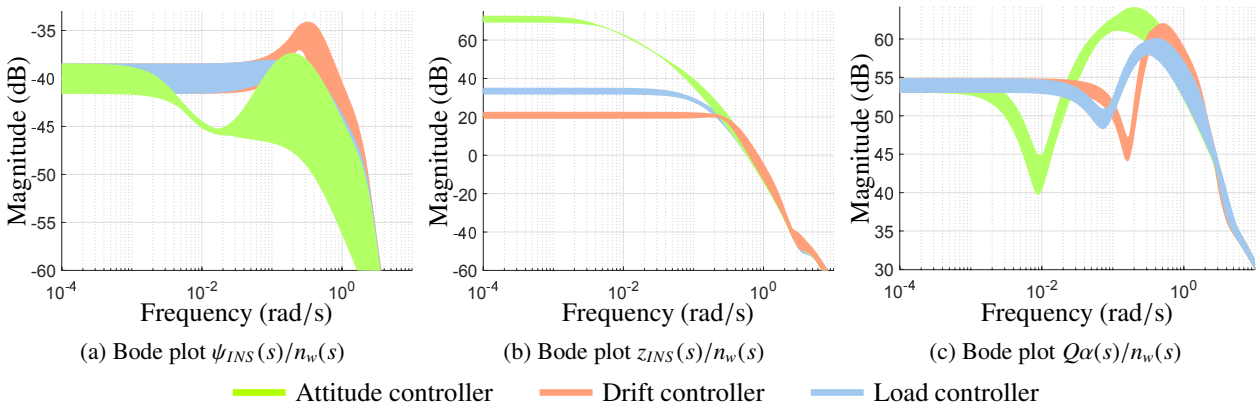

(a) Bode plot $\psi_{INS}(s)/n_w(s)$ (b) Bode plot $z_{INS}(s)/n_w(s)$ (c) Bode plot $Q\alpha(s)/n_w(s)$

Figure 6: Bode plot comparison of attitude, drift and $Q\alpha$ channels from wind disturbance at t=50 s

Finally, Figure 6c shows the frequency responses of the $Q\alpha$-wind channel. In this case, the analysis has to be performed considering frequency ranges since none of the controllers provide best performance across all frequencies. By looking at very low frequencies (between 0.001 and 0.02 rad/s), it is observed that the wind-induced structural loads are further rejected by the attitude controller (in green). However, although the wind disturbance has essentially a low frequency nature, the launch vehicle will also encounter mid- and high-frequency wind gusts. In this regard, it is very clear that the attitude controller will provide a very poor $Q\alpha$ wind disturbance rejection performance for the aforementioned wind gusts. Following on this discussion, for frequencies higher than 0.02 rad/s, the load controller (in blue) is the one providing overall the lowest values, as expected. In this case, the drift controller (in red) further improves the $Q\alpha$-wind performance of the load controller for a small range between 0.1 and 0.3 rad/s, but at the expense of worsening the performance for mid-frequency ([0.02-0.1] rad/s) and high-frequency ([0.3-2] rad/s) wind gusts. To conclude this analysis, it is highlighted that the load controller was not optimised for a specific wind profile, but rather for any wind configuration since it provides good $Q\alpha$-wind rejection performance for low-, mid- and high-frequency wind gusts.

As discussed in sub-section 3.3, in addition to the specific performance design objectives, the different linear controllers are also synthesised to obtain adequate stability margins under dispersed conditions. The stability of the three synthesised controllers is evaluated in Figure 7, which illustrates the Nichols chart at t=50 s of the nominal system (in darker lines) and the same 500 dispersed random LFT samples as before. This plot shows that all designs present satisfactory rigid- and flexible-body stability margins and satisfy all the atmospheric stability requirements (as indicated in reference[14]).

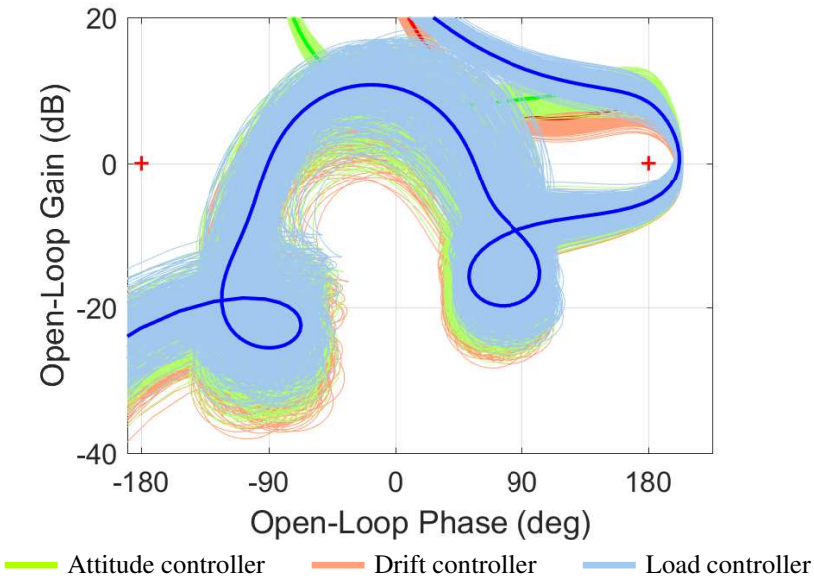

Figure 7: Nichols charts at t=50 s (dispersed stability analysis)

4. Nonlinear trade-off analysis

In this section, the three design control strategies presented above are evaluated using a nonlinear, high-fidelity simulator of the VEGA launcher. This nonlinear analysis is first performed using a Monte Carlo (MC) campaign and a single wind profile (sub-section 4.1). Then, the MC campaign is further extended using 7 different wind profiles (sub-section 4.2) in order to demonstrate that the approach is independent on the specific wind profile used.

4.1 Monte Carlo campaign with the VV05 wind profile

The performance of the attitude, drift and load controllers synthesised in Section 3 are evaluated and compared here using a nonlinear, high-fidelity 6 DoF simulator of the VEGA launcher atmospheric phase. The implementation in the nonlinear simulator is carried out as described in reference.[13] Briefly, a first-order pseudo-derivative filter needs to be added to the TVC architecture to compute the attitude rate error signal $\dot{\psi}_e$. Then, for each control design strategy, all the synthesised linear structured $\mathcal{H}_\infty$ controllers are first discretised using the Tustin's transformation (as discussed in sub-section 3.2.2) with the first bending mode frequency as warping frequency and finally linearly gain-scheduled using the non-gravitational velocity as scheduling parameter. It is noted that this implementation procedure is applied to both pitch and yaw axes.

This nonlinear analysis is based on a MC campaign of 500 runs using the estimated wind encountered in the VEGA VV05 mission.[3] For each run, the same nominal VEGA VV05 flight trajectory is used but more than 125 different system parameters are sampled randomly. The same 500 scattered values are used for the three scheduled global controllers (i.e. attitude, drift and load) in order to perform a fair comparison. Note that theses 500 random samples are different than the ones used in Figure 7 for the stability analysis.

Figure 8 compares the MC attitude error performance (i.e. tracking) for the three analysed controllers. Figure 8a shows the MC responses for both planes, pitch and yaw. Note that the nominal responses are highlighted in darker lines (although they are difficult to appreciate in Figure 8a due to the overlap). As expected, the global attitude controller (in green) provides lower attitude errors than the other two tested controllers throughout the atmospheric flight. This is also noticeable in Figure 8b, which shows for each controller the Gaussian distribution of the (pitch and yaw) attitude error 2-norms computed for each MC run. Note that the 2-norm of each MC response is the square root of the energy, and thus, the lowest 2-norm the better. By looking at Figure 8b, it is clearly seen that the attitude controller presents the lowest attitude error energy (i.e. lowest 2-norm mean), and also the lowest standard deviation (see that it exhibits larger values and thus the distribution is less spread out), which gives a good insight on the robustness of the attitude controller with respect to the tracking performance.

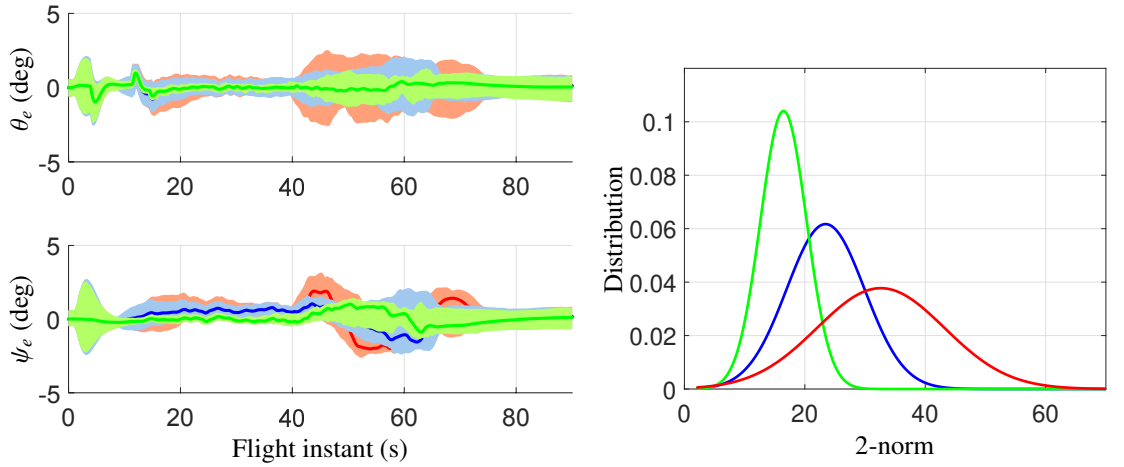

(a) Attitude error Monte Carlo responses

(b) Normal distribution of the attitude-error 2-norm

Attitude controller Drift controller Load controller

Figure 8: Monte Carlo tracking performance analysis using VV05 wind

The MC drift performance is analysed in Figure 9. By looking at Figure 9a, it is observed that the drift controller (in red) achieves the best performance throughout the atmospheric flight. This observation is also confirmed in Figure 9b, where it is shown that the drift controller exhibits less mean and standard deviation than the other two controllers.

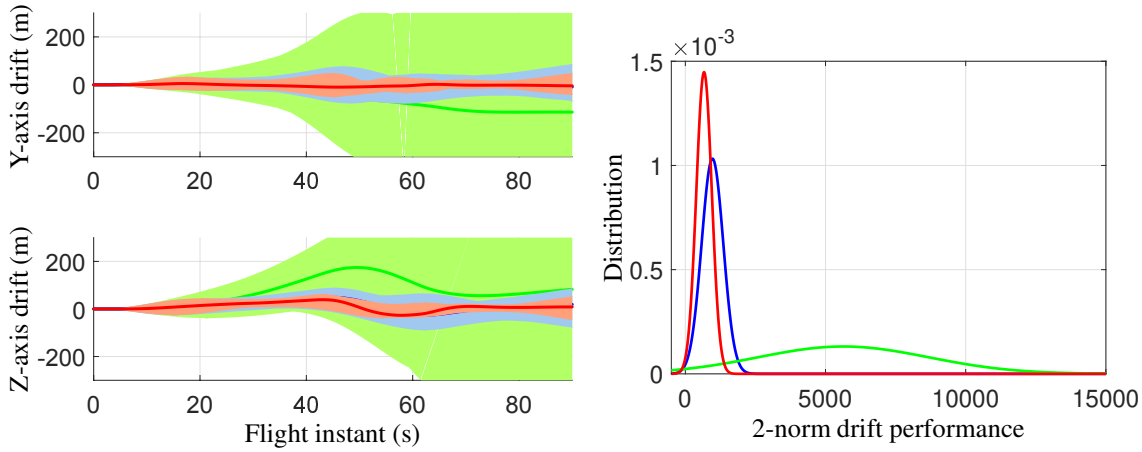

(a) Drift Monte Carlo responses

(b) Normal distribution of the drift 2-norm

Attitude controller Drift controller Load controller

Figure 9: Monte Carlo drift performance analysis using VV05 wind

Figures 8 and 9 clearly highlight the existing trade-off between tracking and lateral deviations. On the one hand, the strategy to minimise the attitude errors is to let the vehicle drift. On the other hand, the drift of the vehicle can be further improved with the consequence of considerably worsening the attitude error performance.

Finally, the same analysis is performed for the structural load performance in Figure 10. The atmospheric-flight TVC system must keep the $Q\alpha$ responses within a given safety envelope depicted in thick dashed-red line in Figure 10a. This plot shows that the three global controllers satisfy this load requirement for all the MC runs. Nevertheless, it is straightforward to see that the attitude controller presents higher $Q\alpha$ peaks along the flight than the other two. This observation is supported by the statistical analysis shown in Figure 10b (see green distribution with higher mean). By comparing the MC responses of the drift and load controllers, it can be inferred that the latter achieves a further reduction of $Q\alpha$ peaks (see Figure 10a between Mach 1.5 and 3) and is also more robust against parametric uncertainties and wind disturbances (i.e. in Figure 10b the load controller exhibits a smaller standard deviation).

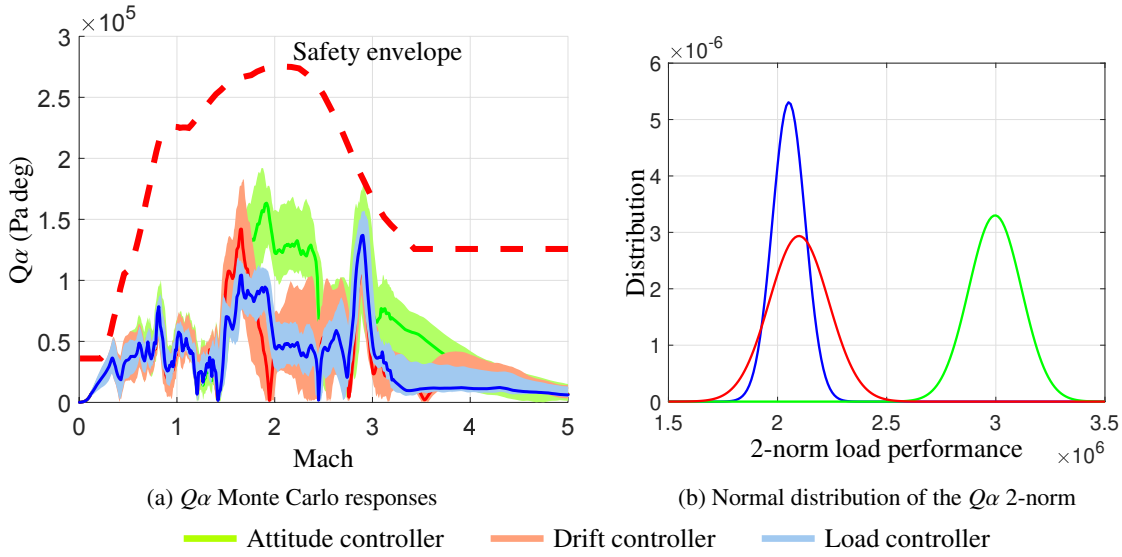

(a) $Q\alpha$ Monte Carlo responses

(b) Normal distribution of the $Q\alpha$ 2-norm

Figure 10: Monte Carlo load performance analysis using VV05 wind

4.2 Monte Carlo campaign with 7 different wind profiles

The nonlinear analysis presented in the previous section is further extended here using 6 more wind profiles. In this instance, 7 MC campaigns of 500 runs (3500 runs in total) are performed for each of the analysed controllers. Each of these MC campaigns uses the same scattering flags employed in the MC campaign of sub-section 4.1 but using a different wind profile. The 7 wind data used for this nonlinear analysis are illustrated in Figure 11, which shows the north and east wind components versus altitude. Note that *Wind A* corresponds to the VV05 wind used in the previous sub-section. The rest have been also obtained from real measurements taken at the VEGA launch site (French Guiana).

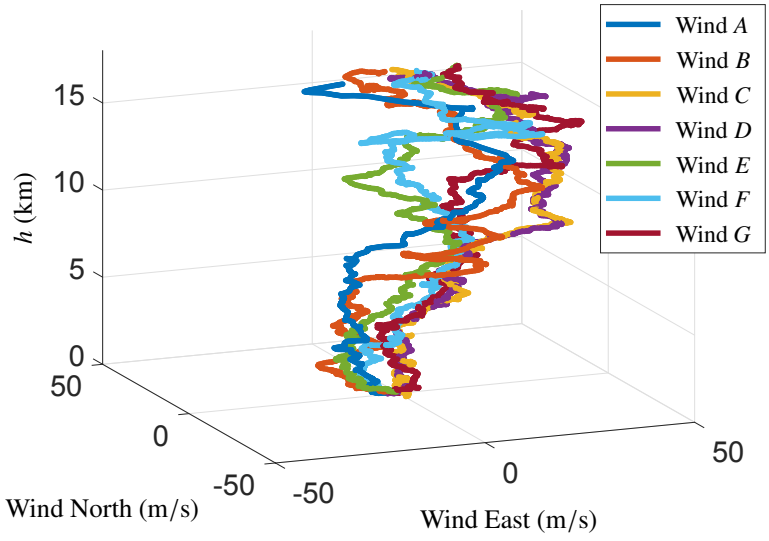

Figure 11: Wind profiles

This MC setup allows to analyse the controllers not only against parametric dispersions but also against moderate and strong wind gusts at different altitudes, and also covering a wide range of wind frequency spectra. The outcomes of this MC campaign are summarised in Figure 12 for four different performance metrics: structural loads, drift, tracking and actuation. As before, the 3500 MC responses of each controller/metric are depicted on the left column, while the 2-norm Gaussian distributions are depicted on the right column.

Figures 12a-b present the MC structural loads performance. By looking at Figure 12a, the first aspect to highlight is the high impact of the wind disturbance on the $Q\alpha$ responses. This plot displays several $Q\alpha$ peaks at different altitudes (or Mach) corresponding to the different wind profiles shown in Figure 11. In this demanding scenario, as expected, the load controller (in blue) attains the best $Q\alpha$ performance. Indeed, the load controller not only achieves lower $Q\alpha$ peaks along the flight envelope in Figure 12a but also better $Q\alpha$ 2-norm statistical properties (i.e. lower mean and standard deviation) as demonstrated in Figure 12b. In addition, it is worth noticing that multiple $Q\alpha$ requirement violations are detected for the drift controller (around Mach 2.5) and for the attitude controller (around Mach 3).

From the drift performance plots (Figures 12c-d), the same conclusions drawn in the previous section are confirmed here for this more challenging analysis setup. The drift controller results in smaller lateral deviations than the other two controllers. Another important observation is that the attitude controller (in green) significantly violates the atmospheric VEGA TVC lateral requirements. In particular, lateral requirement violations (in both position and velocity) are detected in almost half of the 3500 MC runs for the attitude controller. It is noted that the atmospheric VEGA TVC lateral requirements are defined in terms of drift ($z < 500\,\mathrm{m}$) and drift-rate ($\dot{z} < 15\,\mathrm{m/s}$).

As for the attitude error performance in Figures 12e-f, it is very noticeable that the attitude controller successfully minimises the attitude errors with respect to the other two controllers. Similarly as for the analysis in the previous sub-section (recall Figure 8), this feature is distinctly ascertained by looking at the normal distribution in Figure 12f (again, smaller mean and standard deviation). Nevertheless, as discussed before, it is important to remark that this improvement in tracking performance results in critical $Q\alpha$ and drift violations.

Finally, the TVC actuation performance is also analysed here. Figure 12g displays for each controller the 3500 MC TVC actuator deflections in both lanes (A and B). Although less noticeable than in the other analysed performance metrics, it can be inferred that the load control strategy overall requires less TVC deflections and thus provides a reduction on TVC consumption. This aspect is also demonstrated in Figure 12h. This observation is coherent with the physics of the launcher dynamics, since it is reasonable that the other two control strategies require more actuation to follow to reduce the attitude errors and the lateral deviations.

5. Conclusions

This article has illustrated the performance trade-off capabilities that can be achieved for the VEGA launcher TVC design using the methodological approach proposed based on the structured $\mathcal{H}_\infty$ control synthesis algorithm. In particular, the main atmospheric performance requirements were examined: attitude errors, drift and structural loads.

It was shown that the proposed robust scheme can be effectively used to steer the design to favour one of the aforementioned requirements while satisfactorily addressing the classic trade-off between performance and robustness. The results clearly illustrate, via nonlinear, high-fidelity Monte Carlo simulations, the underlying performance trade-off between attitude error and lateral deviations and the required compromise between tracking and drift-rate to minimise the structural loads. These results are indeed achieved by means of a suitable design interconnection reflecting the necessary system dynamics and architectural design, and secondly, of a right formulation of the design objectives via a proper choice of mathematical weighting functions to scale the relative importance of the objectives. Finally, it is highlighted that using the proposed formulation these control strategies can be combined throughout the atmospheric flight to achieve a trade-off balance for the best global performance.

6. Acknowledgments

This work is funded by the European Space Agency (ESA) through the Networking/Partnering Initiative contract No. 4000114460/15/NL/MH/ats. Mr. Diego Navarro-Tapia is also the recipient of a Doctoral Training Partnership award No. 1609551 by the UK Engineering and Physical Sciences Research Council (EPSRC).

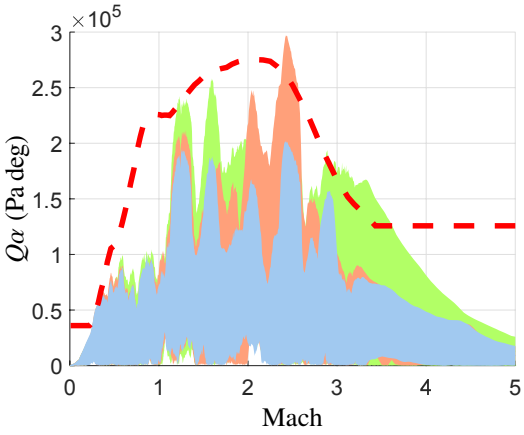

(a) $Q\alpha$ performance

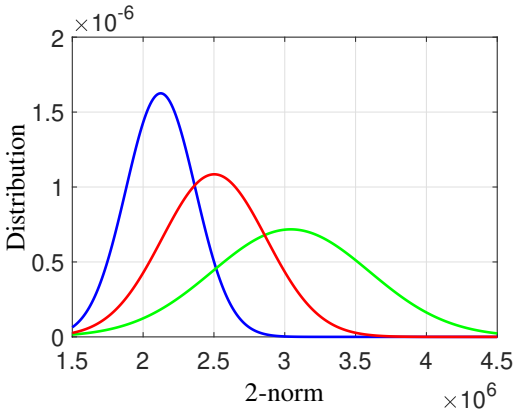

(b) Normal distribution of the $Q\alpha$ 2-norm

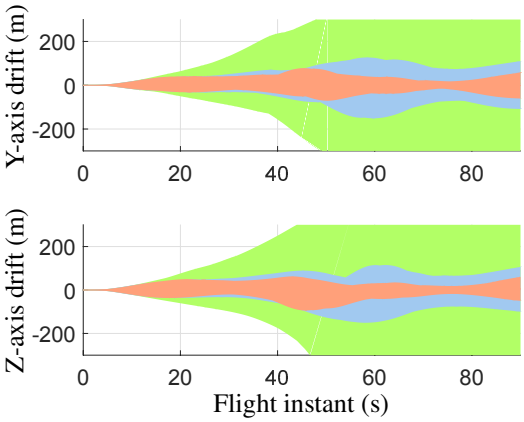

(c) Drift performance

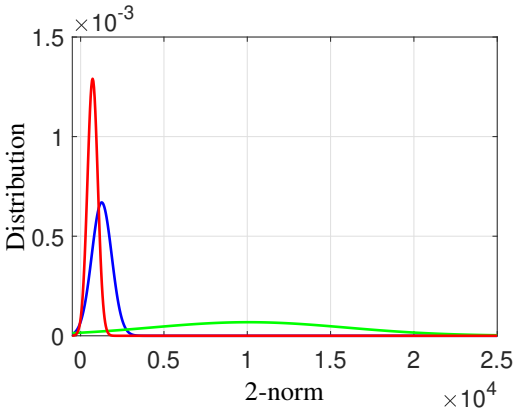

(d) Normal distribution of the drift 2-norm

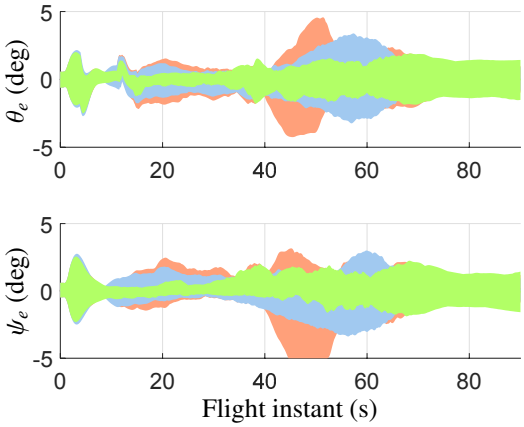

(e) Tracking error performance

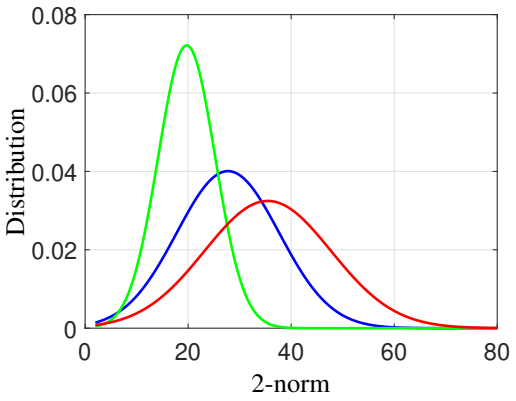

(f) Normal distribution of the attitude error 2-norm

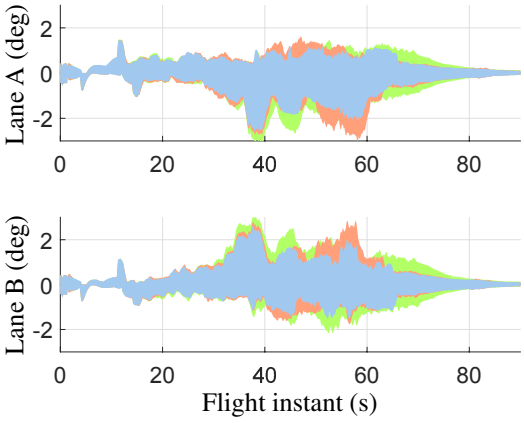

(g) Actuation performance

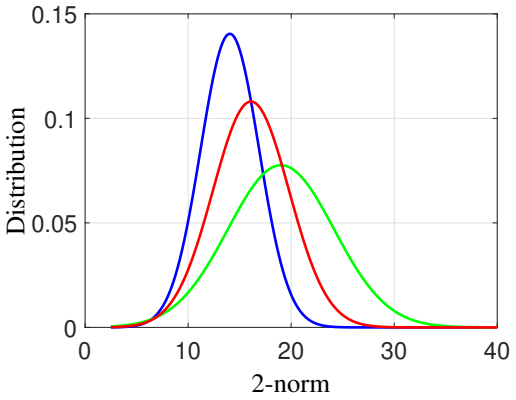

(h) Normal distribution of the actuation 2-norm

Attitude controller Drift controller Load controller

Figure 12: Monte Carlo performance analysis with 7 wind profiles

References

[1] P. Apkarian, M. N. Dao, and D. Noll. Parametric robust structured control design. *IEEE Transactions on Automatic Control*, 60(7):1857–1869, 2015.

[2] P. Apkarian and D. Noll. Nonsmooth $\mathcal{H}_\infty$ synthesis. *IEEE Transactions on Automatic Control*, 51(1):71–86, 2006.

[3] Arianespace. VEGA flight VV05, June 2015. http://www.arianespace.com/mission/vega-flight-vv05/.

[4] G. J. Balas, R. Chiang, A. Packard, and M. G. Safonov. *Robust Control Toolbox*. The MathWorks, Inc., 2005.

[5] D. Sánchez de la Llana, S. Bennani, I. Cruciani, and J. Aranda. H-infinity control of the VEGA launch vehicle first stage in presence of roll. In *Proceedings of the* 19^{th} *IFAC Symposium on Automatic Control in Aerospace*, volume 46, pages 54–59, September 2013.

[6] J. C. Doyle, A. Packard, and K. Zhou. Review of LFTs, LMIs, and μ. In *Proceedings of the* 30^{th} *IEEE Conference on Decision and Control*, pages 1227–1232, December 1991.

[7] P. Gahinet and P. Apkarian. Structured $\mathcal{H}_\infty$ synthesis in MATLAB. In *Proceedings of the* 18^{th} *World Congress of the International Federation of Automatic Control (IFAC)*, volume 18, pages 1435–1440, August 2011.

[8] M. Ganet-Schoeller, J. Desmariaux, and C. Combier. Structured control for future european launchers. *AerospaceLab Journal*, (13):1–10, September 2017.

[9] R. F. Hoelker. *Theory of Artificial Stabilization of Missiles and Space Vehicles with Exposition of Four Control Principles*. NASA Technical Note, NASA TN D-555, June 1961.

[10] D. L. Johnson. *Terrestrial Environment (Climatic) Criteria Guidelines for Use in Aerospace Vehicle Development*. NASA Technical Memorandum, NASA TM 4511, August 1993.

[11] A. Marcos, S. Bennani, C. Roux, and M. Valli. LPV modeling and LFT uncertainty identification for robust analysis: application to the VEGA launcher during atmospheric phase. In *Proceedings of the* 1^{st} *IFAC Workshop on Linear Parameter Varying Systems*, October 2015.

[12] G. F. McDonough, W. D. Murphree, J. C. Blair, J. R. Scoggins, T. G. Reed, E. L. Linsley, V. S. Verderaime, J. A. Lovingood, M. H. Rheinfurth, and R. S. Ryan. *Wind Effects on Launch Vehicles*. Technivision Services, 1970.

[13] D. Navarro-Tapia, A. Marcos, S. Bennani, and C. Roux. Joint robust structured design of VEGA launcher's rigid-body controller and bending filter. In *Proceedings of the* 69^{th} *International Astronautical Congress*, October 2018.

[14] D. Navarro-Tapia, A. Marcos, P. Simplício, S. Bennani, and C. Roux. Legacy recovery and robust augmentation structured design for the VEGA launcher. *International Journal of Robust and Nonlinear Control*, March 2019.

[15] C. Roux and I. Cruciani. Scheduling schemes and control law robustness in atmospheric flight of VEGA launcher. In *Proceedings of the* 7^{th} *ESA International Conference on Spacecraft Guidance, Navigation and Control Systems*, June 2008.

[16] P. Simplício, S. Bennani, A. Marcos, C. Roux, and X. Lefort. Structured singular-value analysis of the VEGA launcher in atmospheric flight. *Journal of Guidance, Control, and Dynamics*, 39(6):1342–1355, 2016.

[17] P. Simplício, A. Marcos, and S. Bennani. New control functionalities for launcher load relief in ascent and descent flight. In *Proceedings of the* 8^{th} *European Conference for Aeronautics and Aerospace Sciences*, July 2019.

[18] H. Suzuki. Load relief control of H-IIA launch vehicle. In *Proceedings of the* 16^{th} *IFAC Symposium on Automatic Control in Aerospace*, pages 985–990, June 2004.

[19] B. Wie, W. Du, and M. Whorton. Analysis and design of launch vehicle flight control systems. In *Proceedings of the AIAA Guidance, Navigation and Control Conference and Exhibit*, August 2008.